PPP Range Error Integrity Using a Network of Ground Monitors

Yu-Fang Lai, Juan Blanch, Todd Walter
Stanford University

BIOGRAPHY

Yu-Fang Lai is a Ph.D. candidate at Stanford GPS Lab. He received Bachelor's degree in Aero/Astro from National Cheng-Kung University in 2020, and Master's degree in Aero/Astro from Stanford in 2022.
Juan Blanch is a senior research engineer at Stanford University. He is a graduate of Ecole Polytechnique in France, he holds an M.S. degree in electrical engineering and a Ph.D. degree in aeronautics and astronautics from Stanford University.
Todd Walter is a Professor at Stanford University and the faculty of Stanford GPS Lab. He received his B.S. degree in physics from Rensselaer Polytechnic Institute and his Ph.D. degree in 1993 from Stanford University.

ABSTRACT

Autonomous vehicles would greatly benefit from a Precise Point Positioning (PPP) service that could support safety critical applications. This paper introduces an integrity monitor system that can provide the (pseudo)range error statistics, range error bias and standard deviation, from a centralized fault-tolerant PPP filter that based on Extended Kalman Filter (EKF). It can process measurements from multiple receivers at different locations.We consider the possibility of receiver faults for the integrity monitor, and form subsets of statistics using Solution Separation (SS) technique similar to Advanced Receiver Autonomous Integrity Monitoring (ARAIM). A robust error characterization is obtained from the subset solutions. As an application of this algorithm, we show that it is possible for geometric error to mask geometric-free error if a clock fault and an ephemeris fault occur at the same time, and how the test statistics from the central filter can successfully resolve this issue.. Finally, we used the fault-tolerant central filter to evaluate GPS fault on PRN-1 (SVN-63) on July 10th, 2023, and compute the robust range error statistics.

I. INTRODUCTION

Single Point Positioning (SPP) relies on the temporal and spatial relation of the receiver to estimate the user position and receiver clock bias. It requires longer time of convergence but can achieve 1$\sim$3 m of position accuracy by applying corrections from navigation message. Precise Point Positioning (PPP) is essentially SPP with the external corrections such as precise satellite clock bias and precise ephemeris. PPP can achieve centimeter level accuracy for static, and decimeter for dynamic receiver. Providing precise corrections to the PPP user and ensuring the integrity of the corrections (especially precise satellite clock bias and precise ephemeris) is the key aspect of PPP service.

While the centimeter/decimeter level of accuracy from PPP is desired and crucial to many applications such as autonomous vehicle, precise guidance in complex environment, drone delivery etc, the safety critical requirement of the PPP service is also important. In particular, the integrity of the user position solutions need to be protected.

Advanced Receiver Autonomous Integrity Monitoring (ARAIM) protects the user integrity by including all signals of constellations that are in-view to the user, then perform Fault Detection and Exclusion (FDE) based, for example, on Solution-Separation (SS) of the measurements. In Blanch et al. (2015), the Protection Level (PL) and Alert Limit (AL) of the snapshot solution is computed to determine whether the user integrity is endangered and which measurements should be excluded to meet Federal Aviation Administration (FAA) requirements for civil aviation. Similar approach can also be applied to PPP in kinematic scenario, (Gunning et al., 2018) performs SS by running a bank of PPP filters in parallel, and each of the filter has measurement exclusion. The PL computation is performed using the estimation from these subset filters.

ARAIM allows single user to do FDE and PL computation independently without external assistance, but it requires extra computations for PL and FDE. The computations grow in factorial if multiple exclusions are needed for small Probability of Hazardously Misleading Information (PHMI) budget. This is a huge computation burden on the user side. As a result, an integrity monitor system that can ensure the integrity of the users is important in a PPP service, that the users of such PPP service can trust their position solution without applying ARAIM on their own solution in a way that the satellites and correction faults have already been monitored. In the previous work (Lai et al., 2023), we constructed the prototype of the integrity monitor system where a fault-tolerant PPP filter is established using Extended Kalman Filter. It introduced the concept of detection state, where an extra free state with high process noise is added to the measurement/satellite we want to monitor. The detection

state is a scalar and functions as an estimate to any unmodelled range error that universally present on a satellite and to all receivers regardless of the receiver locations, and such geometric-free range error is satellite clock bias error. Ideally, the precise satellite clock bias correction provided from the PPP service would eliminate the satellite clock bias, and the expected value of the detection state should be near zero. Therefore, by examining the value of the detection state, we can conclude if there is any satellite clock fault or correction fault happen in real-time and then decide which satellite should be excluded from the users. However, the scalar detection state only considers the faults that are invariant to the geometry of the satellite, and would potentially miss-detect in case of geometry faults. This phenomenon is illustrated in Sec.V.

In this paper, we expand the definition of detection state to include the ephemeris fault, so as to account for the geometric fault. In addition to estimating the satellite clock bias, we also estimate the ephemeris error of the satellite using a centralized filter that takes measurements from multiple receivers from different places at the same time. The resulting estimate of detection state then projects to an arbitrary position to compute the range error contributed from both satellite clock bias and ephemeris error, two of most important corrections in the PPP service. The range error and the associated standard deviation forms the basic statistics for the robust range error for the PPP users.

A significant assumption is that there is only one satellite fault occurring at a time, and we consider the relation between one satellite and multiple receivers. The possibility of receiver fault is also considered and we use SS that is similar to ARAIM but with receiver exclusions. In other words, the integrity of the PPP users is guaranteed with the PPP integrity monitor, and the integrity of the monitor itself is protected by formulating SS to provide statistics that are robust to potential receiver faults.

II. IGS DATASET

The International GNSS Service, IGS (2023), has 515 GNSS receiver stations world-wide as of Nov. 23th 2023 and it provides free access to various GNSS products. The number of stations available may vary from days to days due to new stations introduced, old stations retired, maintenance or events such as power outage.

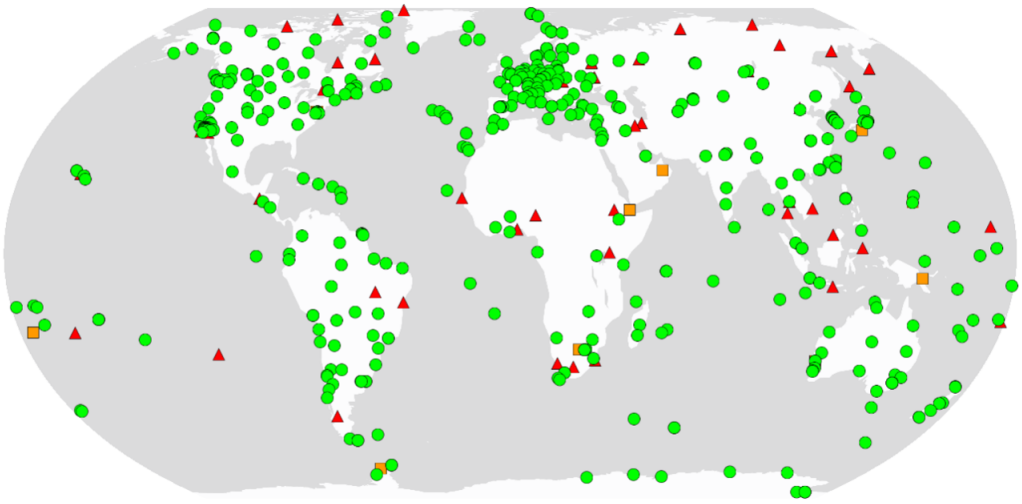

Figure 1: IGS Map and stations. IGS (2023)

In this paper, we used 30(s) interval GNSS measurements from IGS receivers and precise GNSS products, including precise ephemeris (.SP3 file), precise satellite clock bias (.CLK file), Differential Code Bias (.BIA file), Antenna Phase Center Offset (.ATX file) and the estimated receiver position as prior obtained from precise solution (.SNX file).

III. PPP FILTER

The PPP filter in this paper uses Extended-Kalman Filter (EKF) with slight modification to achieve PPP accuracy. We use Joseph Formula (Bucy and Joseph, 2005) for the covariance update to reduce numerical errors and preserve the symmetry of covariance matrix. The measurements of the filter include both code and carrier phase from the GNSS receiver.

A standard PPP filter with static receiver can define its state as:

$$\overrightarrow{x} = \begin{bmatrix} x \\ y \\ z \\ b \\ \nabla b \\ \nabla \hat{T} \\ A^{(1)} \\ \vdots \\ A^{(k)} \end{bmatrix} \tag{1}$$

where $\overrightarrow{x}$ is the state of the filter with single receiver, x, y, z are the receiver position in Earth Centered Earth Fixed (ECEF) coordinate, b is the receiver clock bias, ∇b is rate of change of the clock bias, called clock drift, $\nabla \hat{T}$ is the tropospheric wet delay offset in zenith direction of the receiver, $A^{(k)}$ is the float ambiguities of k^{th} carrier phase measurement. In the case of integrity monitor, the priors are the GNSS receiver being static and we know the true position of the receiver, so we can constrain x, y, z to be fixed to make the estimation of other state more accurate. This is the only constraint we made to the filter throughout the paper.

The measurement models for the PPP filter are dual-frequency code and carrier phase pseudorange.

The Iono-Free (IF) measurement models are defined as follow:

$$\rho_{\text{IF}}^{(i)} = \| \overrightarrow{x}_s^{(i)} - \overrightarrow{x}_{rx} \| + \left(b - b_s^{(i)} \right) + m^{(i)} \nabla \hat{T} + R_m + \epsilon^{(i)} \tag{2}$$

$$\phi_{\text{IF}}^{(i)} = \| \overrightarrow{x}_s^{(i)} - \overrightarrow{x}_{rx} \| + \left(b - b_s^{(i)} \right) + m^{(i)} \nabla \hat{T} + A^{(i)} + R_m + \epsilon^{(i)} \tag{3}$$

where $\rho_{\text{IF}}^{(i)}$ is the ionospheric-free code phase measurement from i$^{\text{th}}$ satellite, $\overrightarrow{x}_s^{(i)}$ is the ephemeris of i$^{\text{th}}$ satellite, $b_s^{(i)}$ is the satellite clock bias, $m^{(i)}$ is the mapping function of tropospheric delay error and ϵ is the un-modelled errors. $\phi_{\text{IF}}^{(i)}$ is the carrier phase ionospheric-free measurement. R_m consists all the modelled effects for both code and carrier phase, which include satellite antenna phase center offset, relativistic effects, solid earth tide modeling, ocean loading, modeled tropospheric delay, Sagnac Effect, phase wind up for carrier phase measurements and differential code bias. Notice the ionospheric-free measurements are computed from dual-frequency measurements, and no single frequency measurements are used in the estimation, so no ionospheric delay model is required for first-order ionospheric error, and all terms are converted to meter. This model does not consider the effect of multi-path.

1. The Detection State

To monitor the satellite clock bias and ephemeris of the satellite of our interest, we define the detection state such that it is added to the measurements from the target satellite. The addition of detection state allows us to evaluate the evolution of the pseudorange error from that satellite and provide statistics to make exclusion decision to the user.

$$\overrightarrow{D_j} = \begin{bmatrix} \zeta_j \\ \Delta \overrightarrow{\gamma}_j \end{bmatrix} \tag{4}$$

The detection states $\overrightarrow{D_j}$ consists two components, where ζ_j corresponds to the satellite clock bias error on j$^{\text{th}}$ satellite and $\Delta \overrightarrow{\gamma}_j$ is a 3×1 vector, the ephemeris error estimate of the j$^{\text{th}}$ satellite. $\Delta \overrightarrow{\gamma}_j$ can be further decompsed into:

$$\Delta \overrightarrow{\gamma}_j = \begin{bmatrix} \Delta x_j \\ \Delta y_j \\ \Delta z_j \end{bmatrix} \tag{5}$$

where $\Delta x_j, \Delta y_j, \Delta z_j$ are defined as the displacement of the j$^{\text{th}}$ satellite position in ECEF coordinate.

Assuming we want to monitor the j$^{\text{th}}$ satellite, the measurement models can be written as:

$$\rho_{\text{IF}}^{(j)} = \| \overrightarrow{x}_s^{(j)} - \overrightarrow{x}_{rx} + \Delta\overrightarrow{\gamma}_j \| + \left(b - b_s^{(j)} \right) + m^{(j)} \nabla \hat{T} + R_m + \zeta_j + \epsilon^{(j)} \tag{6}$$

$$\phi_{\text{IF}}^{(j)} = \| \overrightarrow{x}_s^{(j)} - \overrightarrow{x}_{rx} + \Delta\overrightarrow{\gamma}_j \| + \left(b - b_s^{(j)} \right) + m^{(j)} \nabla \hat{T} + A^{(j)} + R_m + \zeta_j + \epsilon^{(j)} \tag{7}$$

where the satellite clock bias error ζ_j and ephemeris error $\Delta\overrightarrow{\gamma}_j$ are added to the measurement models of the j[th] satellite. All the other measurements follow the standard model we defined in eq.2 and 3. For instance, if we want to monitor the satellite clock bias error and ephemeris error of PRN-1 satellite, eq.6 and 7 are used for measurement from PRN-1 and eq.2 and 3 are used for measurements from other satellites.

Since we have no prior knowledge about what types of faults could happen on satellite clock and ephemeris, the detection state is reset to zero in every time-update and have relatively large process noise to account for the uncertainties of faults. In other words, the detection state is re-estimated in each time-update and are independent to the state in the past.

We monitor the the j[th] satellite clock bias and ephemeris errors by adding the detection state, $\Delta\overrightarrow{\gamma}_j$, which introduces 4 additional parameters to the filter. The spatial parameters $\Delta\overrightarrow{\gamma}_j$ is unobservable if we have less than 3 distinct line-of-sight information from the receiver, where we can only have one from a single receiver. The fact that we are also estimating the on-board satellite clock bias error leads to requiring at least 4 addition receivers for the integrity monitor filter to have meaningful estimate of the detection state. This is analogous to it requires at least 4 satellites to estimate the receiver position and receiver clock bias. In stead, here we estimate the satellite position error and satellite clock bias error on the ground where the receiver position are known to the filter.

As a result, in order to have meaningful estimation of the detection state in a single filter, and make the system observable, the filter of the integrity monitor have to have measurements from at least 4 receivers, of which all of them are located in different positions to have at least 4 different line-of-sight to the satellite we want to monitor, and the receiver position can be constrained to be fixed.

2. Filters of Integrity Monitor: Central Filter

Similar to the standard PPP filter, we can define the state of a receiver as:

$$\overrightarrow{x_i} = \begin{bmatrix} x_i \\ y_i \\ z_i \\ b_i \\ \nabla b_i \\ \nabla \hat{T}_i \\ A_i^{(1)} \\ \vdots \\ A_i^{(k)} \end{bmatrix} \tag{8}$$

where the definition of $\overrightarrow{x_i}$ is the same as eq.1, and i is the i[th] receiver.

The state of the filter for the integrity monitor can then be defined as:

$$\overrightarrow{x} = \begin{bmatrix} \overrightarrow{x_1} \\ \overrightarrow{x_2} \\ \vdots \\ \overrightarrow{x_i} \\ \vdots \\ \overrightarrow{x_n} \\ \overrightarrow{D_j} \end{bmatrix} \tag{9}$$

where there are n different receivers, $n \geq 4$, position of the receiver x_i, y_i, z_i are constrained to be fixed and the j[th] satellite is monitored.

For code and carrier phase measurements from j^{th} satellite, eq.6 and 7 are used as their measurement models, and all the other measurements use eq.2 and 3. They form a centralized filter that estimates multiple receivers at the same time using measurements located at different places. The detection state is what we want to estimate aside from the receiver specific state.

In summary, the central filter contains at least 4 different receivers, each has different position and collects GNSS measurement independently. The filter combines all measurements from the receivers to estimate the satellite clock bias error and ephemeris error of the desired satellite. The receiver positions are known beforehand and as constraints to the receiver positions. That is, the central filter estimates the receiver clock bias, receiver clock drift, tropospheric wet delay correction, ambiguities per receivers, and the detection state. The resulting estimation of the detection state can then be projected to any location with line-of-sight different from the receivers to obtain the range error contributed from both satellite clock error and ephemeris error.

IV. JULY 10 FAULT AND RANGE ERROR PROJECTION

GPS PRN-1 (SVN-63) experienced several clock faults and anomalies in 2023. Particularly, there was a step fault occurred on GPS PRN-1 on July 10^{th} that results in its retirement on Aug. 10^{th} and SVN-44 was reactivated and operates under PRN-22 as the replacement to PRN-1. The July 10^{th} fault is analyzed in detail in Wang et al. (2024). In this section, we use GPS pseudorange measurements from 6 different receivers during the July 10^{th} fault to evaluate the characteristic of the central filter in actual satellite fault scenario. The 6 receivers are from IGS stations, GODN, HLFX, UNB3, NRC1, VALD and SCH2 respectively. They are located in North-East region of North America as shown in the figure below.

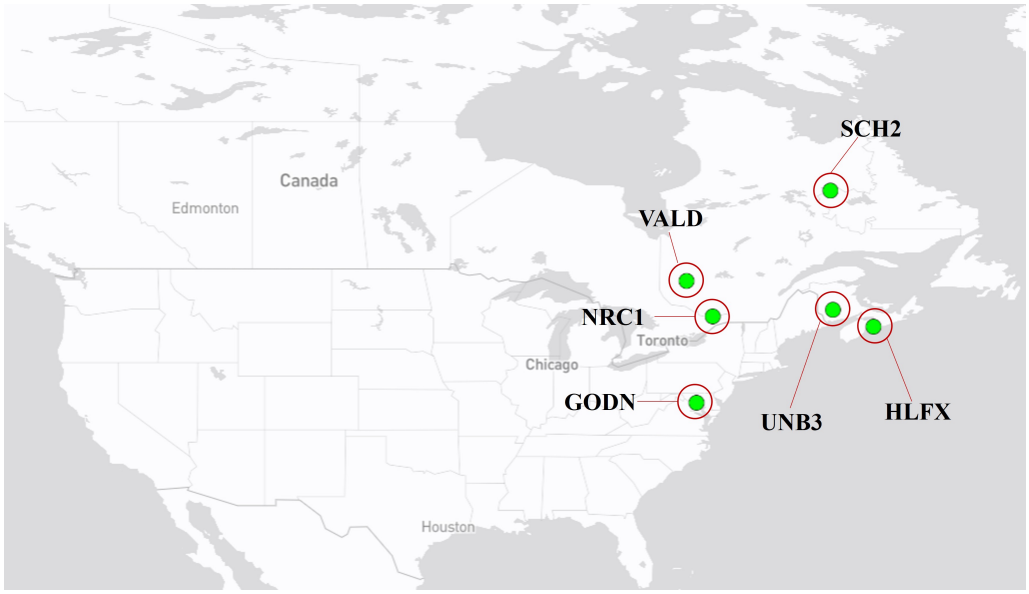

Figure 2: 6 IGS stations used.

1. Satellite Clock Bias Error Only

To investigate the impact of ephemeris error state, we start by having the detection state only estimates the satellite clock bias error.

$$\overrightarrow{D_j} = \zeta_j$$

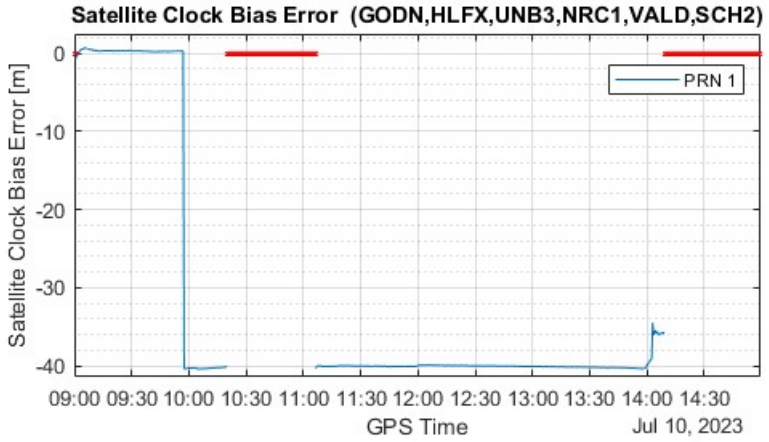

Figure 3: Satellite clock bias error estimate on PRN-1 on July 10th.

Fig.3 is the value of the detection state estimated by the central filter using measurements from the 6 receivers. We can see at $\sim$ 09:57:30 a step fault occurred on GPS PRN-1, causing the estimate of the satellite clock bias error drops to -40 m. From 10:20:30 to 11:06:00 the PRN-1 signal switched to non-standard code so no signals are received from PRN-1 during this period, and are marked as red line in the plot. After 11:06:30, the PRN-1 signal switched back to standard code with un-healthy status. The satellite clock bias error continues to be -40 m until all 6 receivers lost line-of-sight to PRN-1 at around 14:09:00.

The satellite clock bias error estimated by the detection state is the amount of error universally present in the measurements of PRN-1 in all 6 receivers. Regardless of their line-of-sight direction to PRN-1 at the time of satellite clock fault, they were experiencing the exact same range offset. It works as long as the type of fault happened is satellite clock or satellite clock correction, but it would fail to respond if the fault is geometric related, such as ephemeris error.

2. Satellite Clock Bias and Ephemeris Error

The detection state now includes the ephemris error estimate.

$$\overrightarrow{D_j} = \begin{bmatrix} \zeta_j \\ \Delta\overrightarrow{\gamma}_j \end{bmatrix}$$

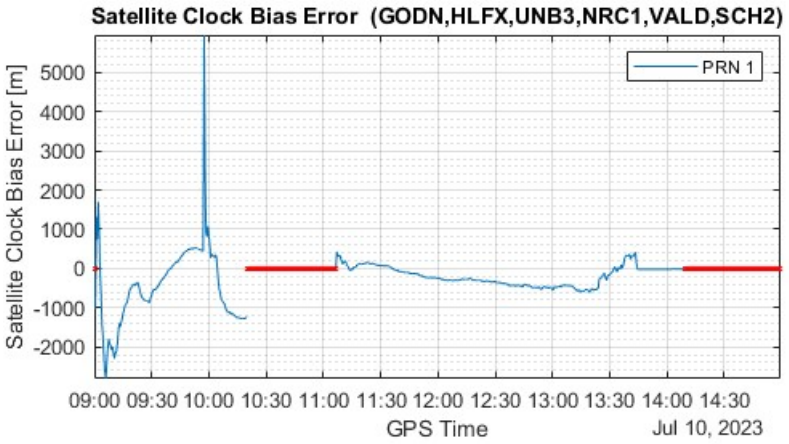

Figure 4: Satellite clock bias error estimate on PRN-1 on July 10th.

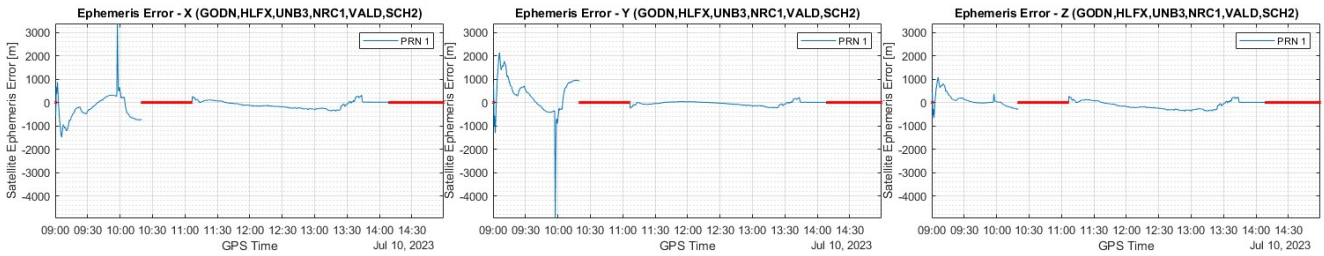

Figure 5: Ephemeris error estimate on PRN-1 on July 10th.

Fig.4 and 5 are the satellite clock bias and ephemeris error estimate from the detection state. The resulting estimate of the ephemeris error on PRN-1 is very noisy, with thousands meters of errors in all 3 directions throughout the estimate. The measurement data and corrections applied are the same as the filter in Fig3. The only difference is the addition of ephemeris error estimate, $\Delta\overrightarrow{\gamma}_j$. The ephemeris state estimates any additional ephemeris error of the monitored satellite, and satellite clock bias state estimates additional common range error amongst the receivers. The direct estimate of the satellite clock bias and ephemeris error is not informative. There was no ephemeris fault on July 10th but the ephemeris estimate shows thousands meters of deviations from the expected zero value. Since the detection states are coupled, the noisy estimate of ephemeris error also affects the estimate of satellite clock bias error, inducing thousands meters of error, where the actual satellite clock bias error is a -40 m.

The reason for the overly noisy estimate of ephemeris error is due to having poor geometry from the 6 receivers. The mutual distances of the receivers are no more than 2000 (km), which are relatively close together comparing to the altitude of PRN-1 satellite, located in MEO orbit of around 20000 (km). The fact that the satellite is moving at around 3.9 km/s also makes it reasonable that the direct estimate of the ephemeris error is noisy.

Although the direct estimate of satellite clock bias and ephemeris error is noisy, what is important for the integrity monitor system is the combined range error (pseudorange error of PRN-1) of the monitored satellite. In this case, the range error at an arbitrary user position, which can be obtained from a simple vector projection of the detection state.

3. Range Error Projection

To demonstrate the range(pseudorange) error after projection, we choose to project the error to the position of the average of the receivers.

The average position of the recievers can be written as:

$$\overrightarrow{x}_{\text{avg}} = \frac{\overrightarrow{x}_{\text{rec},1} + \overrightarrow{x}_{\text{rec},2} + \ldots + \overrightarrow{x}_{\text{rec},n_{\text{rec}}}}{n_{\text{rec}}} \tag{10}$$

The line-of-sight vector from $\overrightarrow{x}_{\text{avg}}$ to the monitored satellite, j^{th} satellite locates at $\overrightarrow{x}^s_j$, is a unit vector:

$$\overrightarrow{l}_{\text{avg},j} = \frac{\left(\overrightarrow{x}^s_j - \overrightarrow{x}_{\text{avg}}\right)}{|\overrightarrow{x}^s_j - \overrightarrow{x}_{\text{avg}}|} \tag{11}$$

The projection of the range error is therefore:

$$\beta_j = \zeta_j + \Delta\overrightarrow{\gamma}_j^{\top} \cdot \overrightarrow{l}_{\text{avg},j} \tag{12}$$

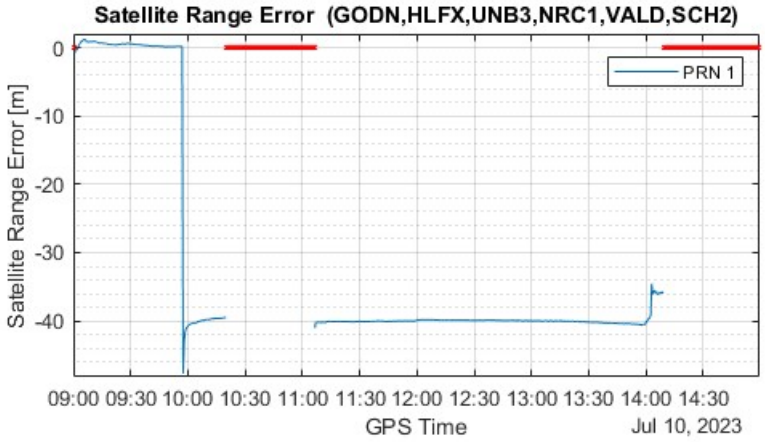

Figure 6: Satellite Range Error on PRN-1 on July 10th.

Fig.6 is the range error of PRN-1 at average receiver position using eq.12 and detection states depicted in Fig.4 and 5. The is the range error estimated by the central filter that considers the effect of satellite clock bias error and ephemeris error. It is shown that the range error is very similar to Fig.3. The overshoot of the range error at 09:57:30 is contributed from the measurements collected by HLFX receiver, where it is previously hidden in the stronger constraints if the detection state considers the range error is equally affected in different receivers. Other part of the range error is slightly different from Fig.3 but can be attributed to the nominal ephemeris error after projection.

The standard deviation of the range error estimate, σ_j, can be computed from taking the covariance of eq.12:

$$\begin{aligned} cov\left(\beta_j\right) &= cov\left(\zeta_j + \Delta\overrightarrow{\gamma}_j^{\top} \cdot \overrightarrow{l}_{\text{avg},j}\right) \\ &= var\left(\zeta_j\right) + var\left(\Delta\overrightarrow{\gamma}_j^{\top} \cdot \overrightarrow{l}_{\text{avg},j}\right) + 2 \cdot cov\left(\zeta_j, \Delta\overrightarrow{\gamma}_j^{\top} \cdot \overrightarrow{l}_{\text{avg},j}\right) \\ &= var\left(\zeta_j\right) + \overrightarrow{l}_{\text{avg},j}^{\top} \cdot var\left(\Delta\overrightarrow{\gamma}_j\right) \cdot \overrightarrow{l}_{\text{avg},j} + 2 \cdot cov\left(\zeta_j, \Delta\overrightarrow{\gamma}_j^{\top}\right) \cdot \overrightarrow{l}_{\text{avg},j} \end{aligned} \tag{13}$$

$$\sigma_j = \sqrt{cov\left(\beta_j\right)} \tag{14}$$

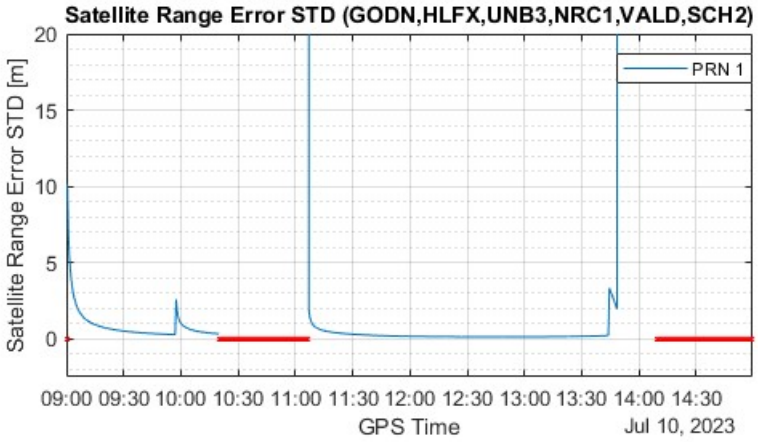

Figure 7: Standard Deviation of Satellite Range Error on PRN-1 on July 10th.

Fig.7 is the standard deviation of the projected range error following eq.13 and 14. The standard deviation of range error rises at 09:57:30 in responses to the step fault, which is corresponding to the start of the -40 m step fault. The initial noise and process noise are set to be extremely high so there are high values of standard deviation at the beginning of the filter and when the PRN-1 measurements reintroduce at 11:06:30. They all quickly converge after few covariance update. The standard deviation rises again at the end of the estimate due to PRN-1 is not in-view to all the receivers.

The central filter can now provide the statistics, β_j and σ_j, to monitor the satellite signals and corrections.

V. EPHEMERIS ERROR MASKING

One potential risk for the central filter to estimate only the satellite clock bias error is it lacks the ability to distinguish the range error contributed by geometric (ephemeris) and geometric-free (satellite clock bias) errors. For example, the ephemeris error might mask the satellite clock bias error such that the range error estimate behaves nominally from the positions of the integrity monitor receivers, which would become a misdetection for users located in other positions and have projection errors that are not exactly canceled.

To demonstrate the risk of ephemeris error masking, we inject a constant ephemeris error to PRN-1 with 40 m magnitude, and direction obtained from the line-of-sight between PNR-1 and HLFX station at 12:30:30, since the 6 receivers are relatively closed to each other so the choice of stations for the direction of ephemeris error does not cause significant differences.

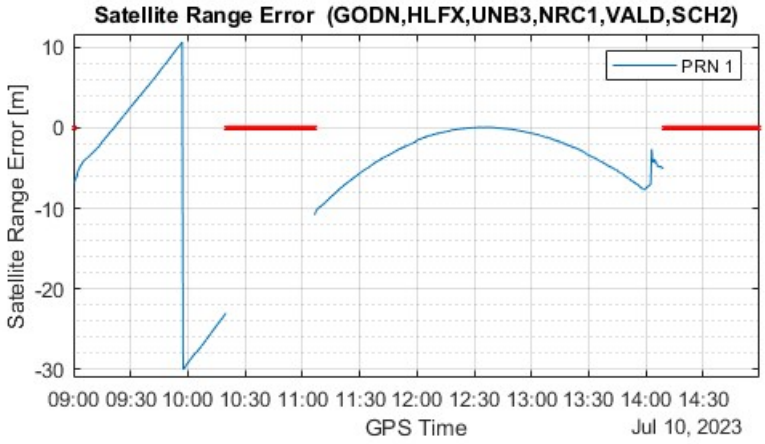

Figure 8: Satellite Range Error on PRN-1 on July 10th with Ephemeris Error Masking. The detection state only estimates satellite clock bias error.

Fig.8 is the estimate of range error projected at average position of the receivers with ephemeris error injection and the -40 m satellite clock bias error. The detection state only contains ζ_j, i.e. $\Delta\overrightarrow{\gamma}_j = \overrightarrow{0}$, so the central filter can only estimate the geometric-free range error from the monitored satellite given the projected error is universally the same according to eq.12. It is shown that the range error estimate is 0 at 12:30:30, which is due to the injected ephemeris error balance the satellite clock bias error. As a result, the integrity monitor filter is unable to detect the fault event if such satellite clock and ephemeris fault happen at the same time as it is at 12:30:30. This is the weakness of estimating the satellite clock bias error alone.

For detection state with both ζ_j and $\Delta\overrightarrow{\gamma}_j$:

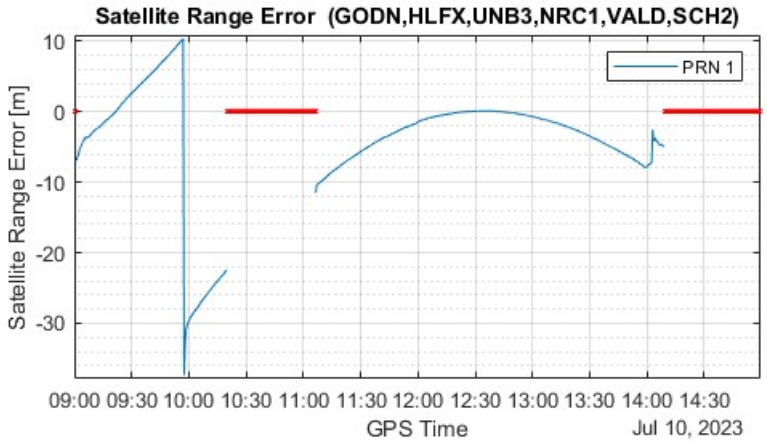

Figure 9: Satellite Range Error on PRN-1 on July 10th with Ephemeris Error Masking.

Fig.9 is the range error of PRN-1 after projecting the detection state to the average of the receiver positions. The projected range error is very similar to Fig.8 and the range error estimate at 12:30:30 is still near zero. As mentioned earlier, the locations of the 6 receivers are very close to each other, so the average position of the 6 receivers are nearly the same from point of view of the PRN-1. The benefit of having ephemeris error estimate is it allows the filter to project the range error to the third place that can be far from the receivers of the measurements.

If the same detection state estimate is projected to the position of INVK station, the IGS station locaced in Inuvik, Canada with latitude, longitude: (68.306°, -133.527°), the range error becomes:

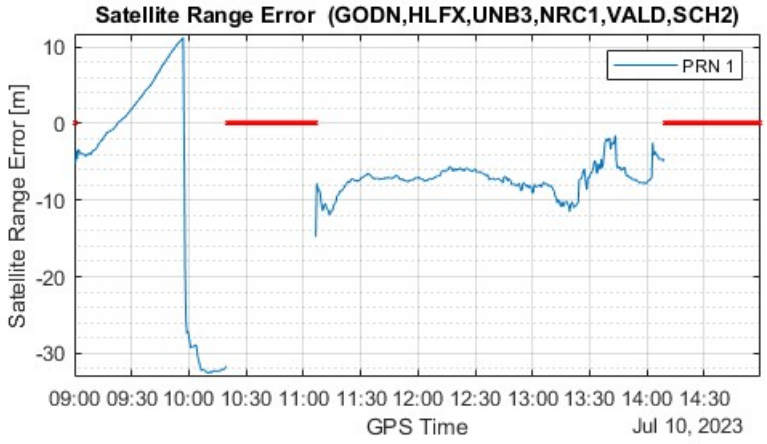

Figure 10: Satellite Range Error Projection at INVK on PRN-1 on July 10th with Ephemeris Error Masking.

Fig.10 is the range error projected to the position of INVK station, using measurements from the 6 receivers. It is clear that at 12:30:30, the effect of ephemeris error injection does not completely remove the -40 m satellite clock bias error. This allows

the integrity monitor to detect the possible risk of having both satellite clock fault and ephemeris fault happen at the same time in a way that the receivers of the monitor are masked.

The computation of the range error is essentially a function of line-of-sight vector. One can project the range error estimate to any place given the satellite is visible to the users to form the statistics for the integrity monitor.

Finally, the projected range error at INVK without the ephemeris error injection is:

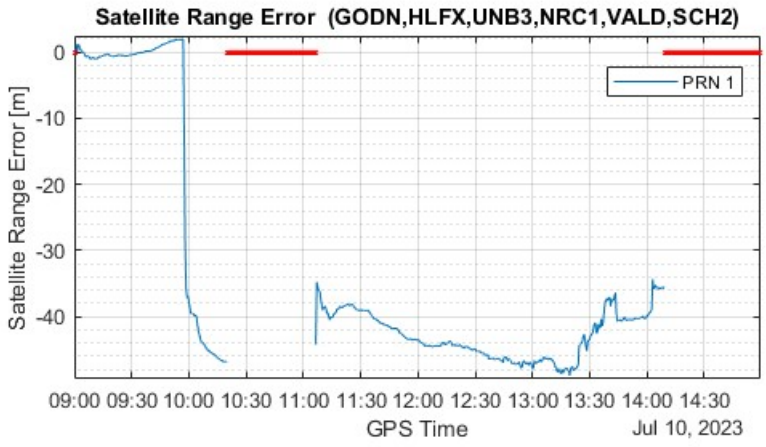

Figure 11: Satellite Range Error Projection at INVK on PRN-1 on July 10th without Ephemeris Error Masking.

Fig.11 is the projected range error at the receiver position of INVK without the injection of ephemeris error. We can see even if the original receivers have poor geometry due to residing too close together, the projected range error can still retain the satellite clock bias estimate at place far from the original receivers. It inevitably becomes noisy due to projecting the range error in the direction with larger covariance.

VI. RECEIVER INTEGRITY

In section IV and V, we established a centralized fault-tolerant filter to be used by the integrity monitor that can monitor the satellite that is in-view to multiple receivers, the projected range error is the combining effect of satellite clock bias error and ephemeris error, and is invariant to the potential ephemeris masking. The resulting output from the monitored satellite and the filter is therefore the range error bias and the associated standard deviation. The bias, β, and standard deviation, σ, form the basic statistics for the integrity monitor, i.e. the projected range error and its standard deviation. They are the local statistics output from the integrity filter. For them to satisfy the integrity and continuity requirement themselves, it is necessary to compute the robust and receiver fault-tolerant statistics to be used in the integrity monitor for satellite fault determination and broadcasting to the user.

In what follows, the subsets are a bank of filter running in parallel, one filter has full access to all measurements and others have various numbers of receiver exclusion. Each filter computes range error statistics assuming satellite clock bias error and ephemeris error from each satellite in-view, and for simplicity it will be referred to as one satellite only so no satellite index is added.

1. Solution Separation: Subset and Receiver Exclusion

Solution Separation (SS) is the optimal way of offering the integrity. It forms subsets of solutions and compares the differences between the solutions to do FDE on satellite measurements. In the prototype integrity monitor, the FDE on satellite measurements and corrections is performed by the central filter and detection state, so what we consider are receiver faults. Similar to Gunning et al. (2018), we can exclude the receiver measurements to form a bank of filters running in parallel, each has different receiver exclusions to account for the possibility of receiver fault.

Each filter provides a pair of unique test statistics after projecting the detection state to a designated position:

$$(\beta_i, \sigma_i) \mid i \in \left\{0, 1, ..., \binom{n_{\text{rec}}}{n_{\text{exclude}}}\right\} \tag{15}$$

i is the index of the subset of receiver exclusion ($i = 0$ indicates no receiver exclusion). n_{rec} is the number receivers and n_{exclude} is the number of exclusions. The number of statistics grows in factorial as number of receivers and exclusions changes.

A simple but conservative way of obtaining the final robust statistics is taking the maximum out of all subsets:

$$\hat{i} = \arg\max_i(|\beta_i|)$$

$$\hat{\beta} = \hat{\beta}_{\hat{i}} \tag{16}$$

$$\hat{\sigma} = \max(\sigma_i) \tag{17}$$

2. Number of Receivers and Exclusions Required for Robust Statistics

The number of receiver exclusions required to have a robust statistics depends on the performance requirement and the number of receivers available to the central filter. Assuming the receiver fault happens independently with probability p_{rec}, a simple model to determine the robustness of the statistics from SS subset is:

$$P\left(n_{\text{fault}} > i\right) = 1 - \sum_{k=0}^{i} \binom{n}{k} p_{rec}^{k} \left(1 - p_{rec}\right)^{n-k} \tag{18}$$

$P\left(n_{\text{fault}} > i\right)$ represents the probability of the number of receiver faults, n_{fault}, is greater than the number of the receiver exclusions, i, so the receiver faults are undetected in the SS subset and are presented in the output statistics. eq.18 can help to determine what subset size is needed to satisfy the performance requirements.

For instance, if the requirement is to have the probability of having receiver fault undetected in the subset solution below PHMI, i.e. $P\left(n_{\text{fault}} > i\right) <$ PHMI, and for PHMI = 10^{-7}, with $P_{\text{rec}} = 0.01$ or $P_{\text{rec}} = 0.00001$:

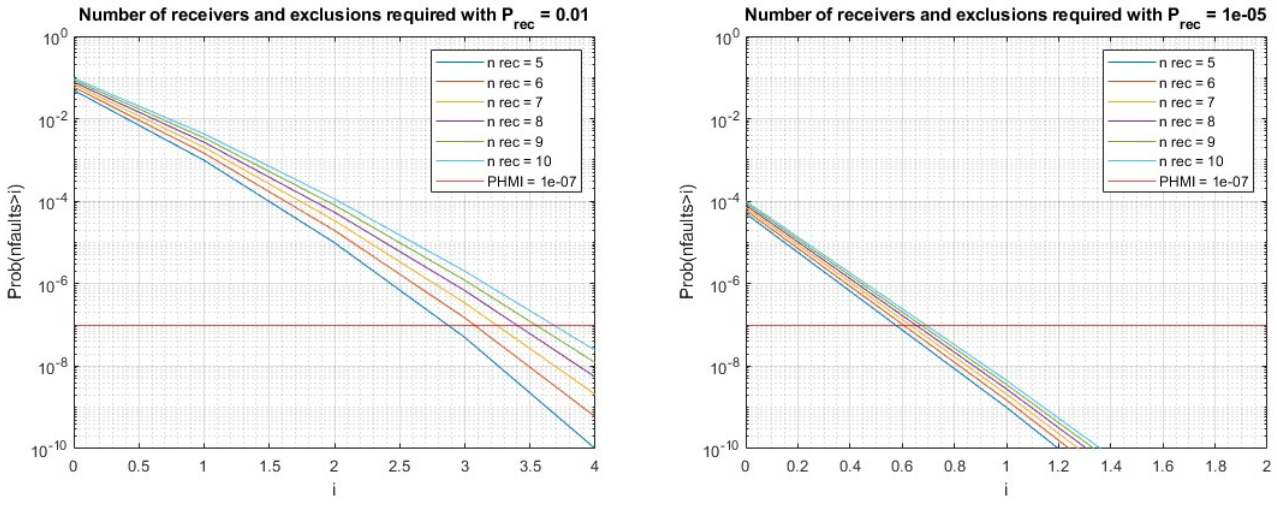

(a) Probability of Receiver Fault = 0.01

(b) Probability of Receiver Fault = 0.00001

Figure 12: Probability of Number of Receiver Faults Greater than Number of Receiver Exclusions.

Fig.12 illustrates the relations between the number of receivers available to the central filter and the number of exclusions needed. The horizontal red line is the value of PHMI = 10^{-7}. For $P_{\text{rec}} = 0.01$ with 5 receivers available, we need to have at least 3 out of 5 receivers excluded in the SS to achieve $P\left(n_{\text{fault}} > i\right)$ below PHMI. Since at least 4 stations are required

to compute the satellite clock bias error and ephemeris error in the central filter, so it does not satisfy the requirement. For $P_{\text{rec}} = 10^{-5}$, the number of exclusions drops to 1, and 5 receivers would suffice in this case. Notice $P\left(n_{\text{fault}} > i\right)$ increases as the number of receivers increases. The more receivers included in the central filter, the more number of receiver exclusions would be potentially required.

3. Conservative Statistics over July 10th Fault

Assume the fault rate of the reciever is $P_{\text{rec}} = 10^{-5}$, so only 1 receiver is excluded in each subset. We can obtain the conservative estimate of the statistics for the July 10th fault:

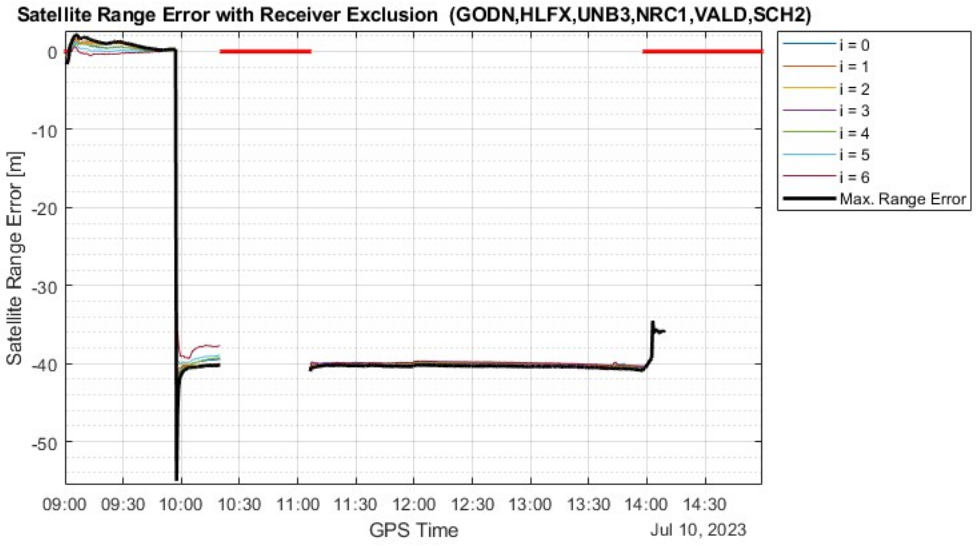

Figure 13: Satellite Range Error Projection at average receivers position on PRN-1 on July 10th with excluding up to 1 receiver.

Fig.13 is the range error estimate of each subset for July 10th fault, with up to 1 receiver being excluded at a time. $i = 0$ is the case where no receiver is excluded. The black line represents the range error with the maximum magnitude among all 7 subsets, which is computed following eq.16. The range error with the maximum magnitude can also be considered as the conservative estimate of the range error for users located at the average receiver positions. This range error estimate satisfies the requirement for having possible receiver fault.

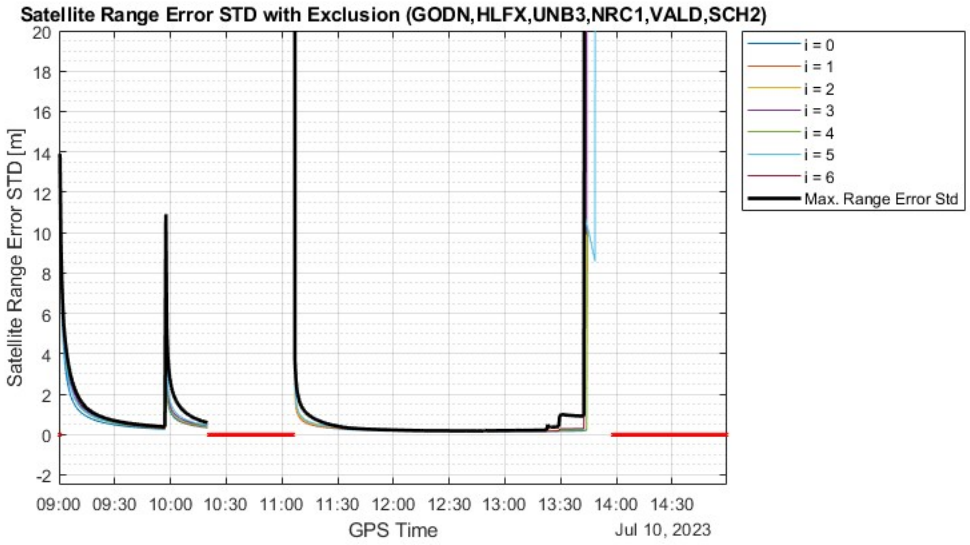

Figure 14: Standard Deviation of Satellite Range Error Projection at average receivers position on PRN-1 on July 10th with excluding up to 1 receiver.

Similarly, Fig.14 is the standard deviation of the range error in different subsets, where $i = 0$ is the case without receiver exclusion. The black line is the maximum of the standard deviation among the subsets. Notice that the range error and the standard deviation are chosen independently, so the conservative statistics may have bias and standard deviation come from different subsets.

The integrity monitor system can then broadcast the robust statistics to users at location near the average position of the receivers, or inform the users not to use measurement from PRN-1 so as to protect the integrity of the PPP service users.

VII. CONCLUSION

We formulated a centralized PPP filter from EKF, that can process dual-frequency GPS measurements collected from GNSS receivers located at different places. We expanded the definition of detection state to include estimation on both satellite clock bias error and ephemeris error. The centralized fault-tolerant filter is capable of monitoring (pseudo)range error by projecting the estimate of the geometric-free (satellite clock bias) and geometric (ephemeris) error state to an arbitrary position, which is chosen to be the average position of the receivers in this paper for convenience. 6 receivers, GODN, HLFX, UNB3, NRC1, VALD and SCH2, from IGS stations are used to evaluate the July 10th fault, which happened on GPS PRN-1 (SVN-63), causing it to have a -40 m of range error during the incidence. It is shown that the central filter can detect the correct range error after projecting the estimate of the detection state to an arbitrary location. We also injected an artificial constant ephemeris error to PRN-1, which would mask the -40 m range error during the incidence. The range error projection can successfully capture the fault by projecting the range error to other places where the satellite clock bias error and ephemeris error are not completely canceled out. Finally, we consider the possibility of having receiver faults. In order to have guarantees on the integrity of the integrity monitor, we followed a similar process as ARAIM. We formed a subset of solution separation filters with receiver exclusion to compute the corresponding conservative statistics that represents the robust range error for the monitored satellite.

ACKNOWLEDGEMENTS

We gratefully acknowledge the support of the Hexagon and NovAtel Inc. for funding this work. We also thank the FAA Satellite Navigation Team for funding this work under Memorandum of Agreement #: 693KA8-22-N-00015.

REFERENCES

Blanch, J., Walker, T., Enge, P., Lee, Y., Pervan, B., Rippl, M., Spletter, A., and Kropp, V. (2015). Baseline advanced raim user algorithm and possible improvements. *IEEE Transactions on Aerospace and Electronic Systems*, 51(1):713–732.

Bucy, R. and Joseph, P. (2005). Filtering for stochastic processing with applications to guidance.

Gunning, K., Blanch, J., Walter, T., de Groot, L., and Norman, L. (2018). Design and evaluation of integrity algorithms for ppp in kinematic applications. In *Proceedings of the 31st International Technical Meeting of the Satellite Division of The Institute of Navigation (ION GNSS+ 2018)*, pages 1910–1939.

IGS, M. (2023). International gnss service.

Lai, Y.-F., Blanch, J., Walter, T., Kahr, E., Leahy, E., Silva, P., and Ellum, C. (2023). Prototyping integrity monitors for ppp fault detections. In *Proceedings of the 36th International Technical Meeting of the Satellite Division of The Institute of Navigation (ION GNSS+ 2023)*, pages 2592–2605.

Wang, R., Lai, F., and Walter, T. (2024). Characterization of the most recent gps satellite fault. In *Proceedings of the 2024 International Technical Meeting of The Institute of Navigation*.